Advances in Science and Technology
ISSN: 1662-0356, Vol. 171, pp 11-24
doi:10.4028/p-O4q45b

Submitted: 2025-06-13
Revised: 2025-07-14
Accepted: 2025-08-05
Online: 2025-12-19

Modelling Vehicular Impact for Threat-Dependent Progressive Collapse Assessments

Gioele Montalbetti[1,a*], Alex Sixie Cao[1,2,b] and Andrea Frangi[1,c]

[1]ETH Zurich, Institute of Structural Engineering
Stefano-Franscini-Platz 5, 8093 Zurich, Switzerland

[2]Empa, Swiss Federal Institute of Materials Science and Technology, Structural Engineering Research Laboratory, Ueberlandstrasse 129, 8600 Dübendorf, Switzerland

[a]Gioele.Montalbetti@ibk.baug.ethz.ch, [b]alex.cao@empa.ch, [c]frangi@ibk.baug.ethz.ch

Keywords: vehicular impact, progressive collapse, chained hazard, notional damage, kinetic energy

Abstract. Structural robustness is vital to prevent disproportionate damage in a progressive collapse of a structure. Current assessment methods in building structures, such as the notional removal of structural members, are unable to capture cascading effects from debris impact loading and chained hazard scenarios. Vehicular impact with penetration into the building volume is an example of a plausible chained hazard scenario. In this study, the adequacy of notional damage methods was assessed for vehicular impact loading on building structures and a comprehensive framework was developed to address key limitations in conventional design methods against vehicular impact. The conventional approaches have relied on prescriptive forces and simplified models and have overlooked important phenomena, such as variable vehicle stiffness and energy dissipation mechanisms. The use of the vehicular impact framework has been exemplified using a model for progressive collapse to assess the consequences of successive time-delayed column loss on the structural response from the penetration of a lorry. The time-delay of successive column loss from vehicular impact was determined by considering the kinetic energy and energy dissipation mechanisms. Higher initial velocities lead to higher post-impact velocities after the initial impact on a column and to a reduction in time between successive failures, thus heightening the likelihood of cascading failures in structural columns and progressive collapse. Progressive collapse simulations revealed that a building structure may have sufficient robustness to prevent progressive collapse when subjected to the loss of single columns. However, successive column losses triggered an extensive progressive collapse.

Introduction

Structural robustness can be defined as the insensitivity of a structure to initial damage caused by events like fire, explosions, impact or the consequences of human error [1]. Ensuring structural robustness is vital to minimising the consequences of progressive collapse. A widely accepted method for assessing the robustness of structures is to impose arbitrary damage through the notional removal of a discrete vertical member [1–3]. However, this method often overlooks chained events, such as debris impact, propagating actions, and sequential failures. Moreover, its implementation is not uniform across different standards [1–3]. The design standards EN 1991-1-7:2006, ASCE/SEI 76-23 and UFC 4-023-03 incorporate different approaches regarding notional damage. EN 1991-1-7:2006 focuses on assessing the sudden removal of individual vertical load-bearing members, such as columns or walls; ASCE 76-23 uses notional damage volumes depending on the risk of the structure and requires the engineer to identify critical locations; UFC 4-023-03 emphasises alternate load paths for specified column and wall removal scenarios and requires enhanced local resistance for all perimeter first-story columns or walls. It is assumed that the arbitrary damage scenarios are adequate surrogates for relevant hazards. However, this abstraction may not be appropriate for some types of hazards. Examples are the systematic damage to several components and chained hazards.

The increasing number of extreme events, such as intentional [4] and unintentional [5] vehicular impact on facilities and infrastructure, highlights the need to deepen the understanding of this hazard and its implications on the built environment. Between the year 2000 and 2020, 31 incidents of

vehicle-based attacks on facilities and infrastructure were recorded [4]. This may seem a low number, but it is multiple times higher with respect to the five incidents recorded in the previous 30 years [4]. Based on data from the Storefront Safety Council [5], vehicle-into-building crashes in the US were 40 % higher than previously thought [6]. More recent events [7] [8] further underline the underestimation of vehicle impacts on buildings. Examples of other incidents include tram collisions into buildings [9] and lorry impacts [10].

For vehicular impact, potential penetration into the building volume may exacerbate the resulting building damage. Current design guidelines and codes primarily address vehicular impacts using prescriptive loads and simplified models [1,11,12]. They typically assume a spring stiffness to determine the impact force resulting from the impulse of an impact [1,11]. For hard impact, the structure is assumed as rigid and the colliding object linear during the impact phase. For soft impact, the structure is assumed elastic and the colliding object rigid [1]. In EN 1991-1-7:2006, prescriptive values for the vehicle stiffness neglects the large variability of vehicles and their properties. Thus, conventional design approaches may not capture the relevant mechanical phenomena, such as dynamic interactions and energy dissipation mechanisms, especially when multiple failures or cascading effects have to be assessed.

To address the gaps, this study presents a framework to determine vehicular impact loads dependent on the vehicle and structural characteristics. The vehicle is modelled with the Campbell model, which is a widely used approach for estimating impact forces and energy dissipation for vehicular impact [13]. This model was chosen for its simplicity and applicability to impulse relations. It uses key parameters, such as the limit of absorbed elastic energy and the distributed stiffness across the vehicle's width. The Campbell model is used in conjunction with classical mechanics to develop velocity and energy profiles as a function of time and distance, complementing existing approaches. The use of the profiles is exemplified on a case study of a lorry penetrating a building. In the case study, the successive loss of multiple columns from the lorry is compared with the loss of a single column using a modelling framework for progressive collapse.

Materials and Method

Vehicle Impact Model. To model the impact forces and energy dissipation on the vehicle side, the Campbell model is used [13]. This model, depicted in Fig. 1a, assumes a constant stiffness over the elastic and plastic region of the load-displacement diagram. The equations are expressed with the residual plastic crush $\bar{c}$, the yield-point stiffness parameter A and the stiffness parameter B [13,14] representing the distributed linear plastic stiffness over the width of the vehicle illustrated in Fig. 1b.

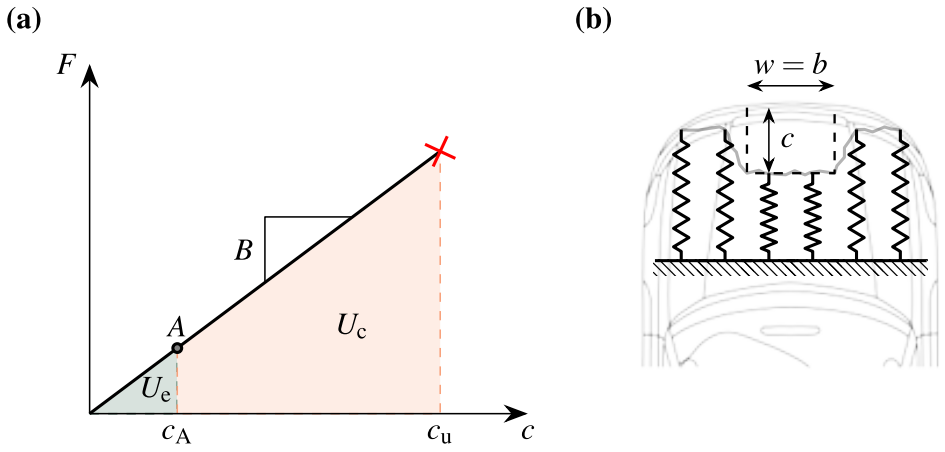

Fig. 1. Campbell model. (a) Constitutive law with crush coefficients [13]. (b) Crush shape assumption.

The impact force F can be directly determined from:

$$F = (A + B\bar{c})w = Bcw, \tag{1}$$

where A and B are crush stiffness coefficients, $\bar{c}$ is the average purely plastic crush, c the total crush and w is the crush width. The values of the crush stiffness coefficients A and B are based on experiments on lorries [15] and the parameters are summarized in Table 1.

By assuming the crushed shape, as depicted in Fig. 1b, the representative vehicle spring stiffness k_v can be calculated by multiplying the linear plastic stiffness coefficient B with the impacting object width b.

$$k_\mathrm{v} = Bw = Bb. \tag{2}$$

If a very wide crush width w is assumed for determining the equivalent vehicle spring stiffness k_v, unrealistically high impact forces could result. The local damage with approximately the width of the impacted object b can be observed in various crash incidents and simulations [16,17]. By rearranging Eq. (1) and expressing the force F as the impact force, the total crush c can be expressed as:

$$c = \frac{P_\mathrm{imp}}{k_\mathrm{v}}, \tag{3}$$

where P_imp is the impact force. The total crush energy U_v, consisting of the elastic energy U_e and plastic energy U_c, is the area under the force-displacement curve shown in Fig. 1a and can be expressed as:

$$U_\mathrm{v} = U_\mathrm{e} + U_\mathrm{c} = \int_0^{c_\mathrm{A}} F(c)dc + \int_{c_\mathrm{A}}^{c_\mathrm{u}} F(c)dc = \frac{1}{2}Fc = \frac{1}{2}k_\mathrm{v}c^2 \tag{4}$$

Table 1. Vehicle characterisation.

Vehicle type	m_v (kg)	A (kN/m)	B (kN/m^2)
Lorry	20 000	45	1 300

Structural impact model and material properties. The structure is idealised as a column pinned at both ends with a linear elastic and perfectly brittle material behaviour. A representation of the static system is shown in Fig. 2. The material is assumed to be glued laminated timber of strength class GL24h according to EN 14080:2013 [18], with the mean material parameters summarised in Table 2. The length of the column L is 3 500 mm. To design the perimeter column cross-section, the deterministic impact force of 500 kN according to EN 1991-1-7:2006 [1] and design level resistance and load values were used. This results in a square cross-section of 500 × 500 mm. Internal columns were not designed for vehicular impact loading and a typical cross-section of 300 × 300 mm was chosen. The spring stiffness k_s at any point z along the column can be expressed as:

$$k_\mathrm{s} = \frac{3EIL}{(L-z)^2z^2}. \tag{5}$$

In this paper, the axial forces of the column are neglected. Therefore, the resistance checks to ensure the structural integrity are performed for pure bending and shear. The bending resistance is:

$$M_\mathrm{R} = \frac{6f_\mathrm{dyn}}{h^2b} \tag{6}$$

where M_R is the flexural resistance, $f_\mathrm{dyn} = k_\mathrm{dyn}f_\mathrm{m}$ is the dynamic bending resistance, k_dyn the force based dynamic strength increase factor [19], f_m the mean bending resistance [20], and h the height and b the width of the column. For a rectangular cross-section, the shear resistance is:

$$V_{\mathrm{R}} = \frac{2}{3}\tau_{\mathrm{dyn}} bh, \tag{7}$$

where V_{R} is the shear force resistance, $\tau_{\mathrm{dyn}} = k_{\mathrm{dyn}} f_{\mathrm{v}}$ is the dynamic shear stress and f_{v} the mean shear resistance calculated based on the JCSS Probabilistic Model Code [21].

Table 2. Material properties of glued laminated timber of strength class GL24h according to Cao and Frangi [19] and Schilling et al. [20]

Material	E_{m} (N/mm^2)	f_{m} (N/mm^2)	f_{v} (N/mm^2)	k_{dynR} (-)	k_{dynE} (-)
GL24h	12 800	32.9	3.27	2.0	3.0

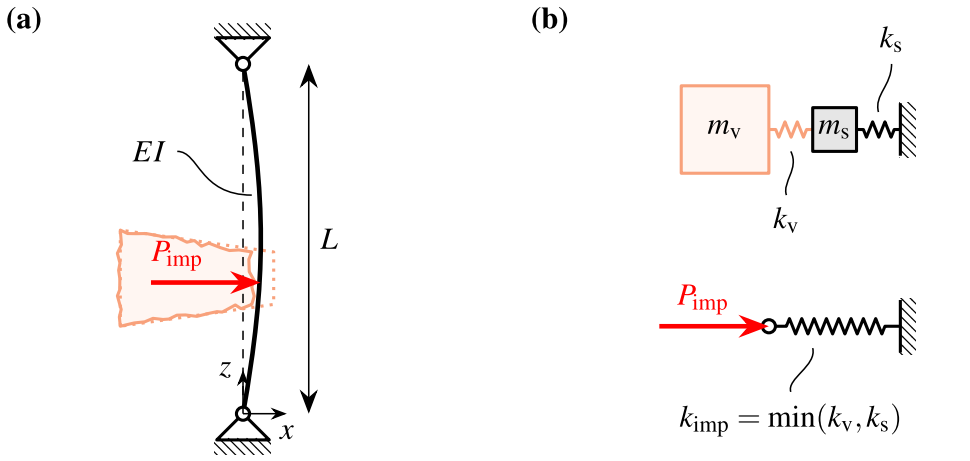

Fig. 2. Static system and modelling simplifications. (a) Column model with boundary conditions and idealised vehicle. (b) Corresponding SDOF models.

From comparing the impulse duration t_{imp} to the natural period T_{n} of the column, $t_{\mathrm{imp}} \gg T_{\mathrm{n}}$. This would suggest that the impact can be treated as quasi-static loading. In reality, it is not a direct representation of the dynamic effects during vehicular impact. There are three main highly dynamic phases, bumper impact with plastic deformation, engine impact with a sudden high impulse, and cargo impact. Therefore, dynamic effects from the analysis are taken into account by an upper limit dynamic amplification factor for linear elastic materials $\phi_{\mathrm{dyn}} = 2.00$ [22]. As such, the dynamic impact load is given by:

$$P_{\mathrm{dyn}} = \phi_{\mathrm{dyn}} P_{\mathrm{imp}}. \tag{8}$$

The maximum acting bending moment M_{S} is expressed with the following relation:

$$M_{\mathrm{S}} = \frac{P_{\mathrm{dyn}}}{L}(L - z)z, \qquad z \le L/2. \tag{9}$$

The maximum shear force is determined using:

$$V_{\mathrm{S}} = \frac{P_{\mathrm{dyn}}}{L}(L - z), \qquad z \le L/2. \tag{10}$$

By combining Eq. (5) and Eq. (8), the dynamic impact load P_{dyn} can be expressed with respect to the bending moment resistance M_{R}:

$$P_{\mathrm{dyn,M}} = \frac{6L}{h^2 b(L-z)z} f_{\mathrm{dyn}} \tag{11}$$

Similarly, this can be performed for the shear force resistance V_{R}:

$$P_{\mathrm{dyn,V}} = \frac{2bhL}{3(L-z)} \tau_{\mathrm{dyn}} \tag{12}$$

By idealising the system as a single-degree-of-freedom system, the elastic strain energy U_{s} can be determined with the spring stiffness k_{s} in Eq. (4):

$$U_{\mathrm{s}} = \frac{1}{2}\frac{P_{\mathrm{dyn}}^2}{k_{\mathrm{s}}} = \frac{P_{\mathrm{dyn}}^2 (L-z)^2 z^2}{6EIL}, \tag{13}$$

with $P_{\mathrm{dyn}} = \min\left(P_{\mathrm{dyn,M}}, P_{\mathrm{dyn,V}}\right)$, depending on whether shear or bending moments are governing. The governing failure mode is used to determine the maximum strain energy capacity U_{s} of the column. Shear is governing if the impacts occurs low on the column. According to EN 1991-1-7:2006, the impact location for lorries may be varied between 0.50 and 1.50 m. In this study, 1.50 m is used. Based on the stated assumptions, bending is generally governing for the performed verifications.

Impact model. The impact scenario is simulated by generating velocity profiles along the trajectory of the vehicle, from the point where it leaves the roadway, to its secondary collision with an internal column. A representation of the procedure is depicted in Fig. 3. Throughout its trajectory, the vehicle is subjected to a deceleration caused by braking forces or encounters with impeding objects. This deceleration results in a reduction in the velocity. The relationship between the initial velocity v_0 and deceleration a can be expressed as:

$$v(x) = \sqrt{v_0^2 - 2ax}, \tag{14}$$

where $v(x)$ is the velocity at every location x due to the initial velocity and deceleration, v_0 is the initial velocity and is considered between 30 and 80 km/h to represent typical circumstances in urban and rural areas, and a the deceleration of 4 m/s2. The deceleration value is based on recommendations from the Joint Committee on Structural Safety [11]. It is assumed that the deceleration outside and inside the building is the same. At impact, the velocity decrease is determined by a reduction in kinetic energy:

$$E_{\mathrm{k},i}^{+} = E_{\mathrm{k},i}^{-} - U_{\mathrm{v}}\left(P_{\mathrm{dyn}}\right) - U_{\mathrm{s}}\left(P_{\mathrm{dyn}}\right), \tag{15}$$

where $E_{\mathrm{k},i}^{+}$ is the kinetic energy of the vehicle post-impact, $E_{\mathrm{k},i}^{-}$ the kinetic energy of the vehicle pre-impact, i are the different impact locations, U_{c} the dissipated energy due to vehicle crush according to Eq. (3) and U_{s} the dissipated strain energy due to strain energy accumulated in the column from Eq. (12). At the initial location of impact $i = 0$, $E_{\mathrm{k},i}^{-}$ is expressed as:

$$E_{\mathrm{k},0}^{-} = \frac{1}{2} m_{\mathrm{v}} v^2 = \frac{1}{2} m_{\mathrm{v}} (v_0^2 - 2as), \tag{16}$$

where s is an assumed braking distance s of 4 000 mm, which represents walkways and other free surfaces between streets and buildings

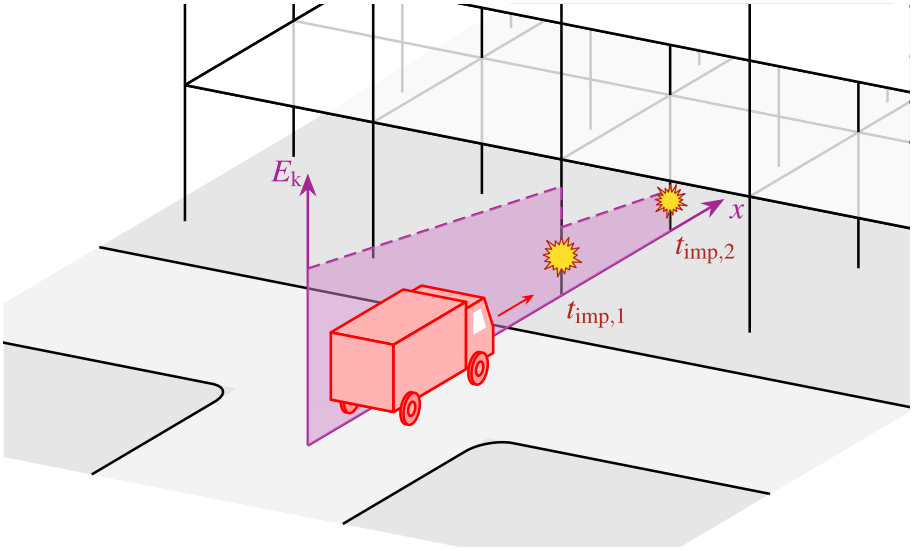

Fig. 3. Kinetic energy profile of a vehicle driving into a building.

To evaluate the crush c and strain energy U_s, the impact load P_{imp} must be determined. The vehicle's impulse can be expressed with the force-impulse relation $\mathcal{I} = \int_t P dt = m_v v$. By assuming a pulse shape, the impact duration Δt_{imp} can be determined from the maximum impact load P_{imp} and impulse $m_v v$ of the vehicle. The interaction between the vehicle and the structure during the impact is governed by the effective spring stiffness k_{imp}. In this paper, it is assumed that the spring stiffnesses $k_{\{v,s\}}$ are dissimilar to an extent that considering only the minimum is a good approximation:

$$k_{imp} = \min(k_v, k_s), \tag{17}$$

where k_v is the spring stiffness of the vehicle and k_s the spring stiffness of the column. A similar assumption is made in EN 1991-1-7:2006. A representation of the idealised single-degree-of-freedom (SDOF) model is depicted in Fig. 2b. With the assumption of a triangular pulse, the impact load P_{imp} becomes.

$$P_{imp} = v_{imp}\sqrt{k_{imp} m_v}, \tag{18}$$

where v_{imp} is the vehicle velocity and m_v the vehicle mass. With a triangular pulse and linear behaviour, the impact duration t_{imp} becomes [23]:

$$t_{imp} = 2\sqrt{\frac{m_v}{k_{imp}}}. \tag{19}$$

The pulse shape and force-impulse relation is illustrated in Fig. 4. A triangular pulse shape leads to longer impact times with respect to a rectangular impulse shape and a rectangular pulse shape is also incompatible with a linear response [22]. If the dynamic impact load is $P_{dyn} \leq \min(P_{dyn,M}, P_{dyn,V})$ the vehicle is arrested and the velocity profile beyond the initial impact is 0. If the dynamic impact load is $P_{dyn} > \min(P_{dyn,M}, P_{dyn,V})$, the column fails and the reaction-based dynamic strength increase coefficient k_{dynR} is substituted by the energy based dynamic strength increase factor k_{dynE} accounting for the energy dissipated after the peak resistance assuming full rupture [19].

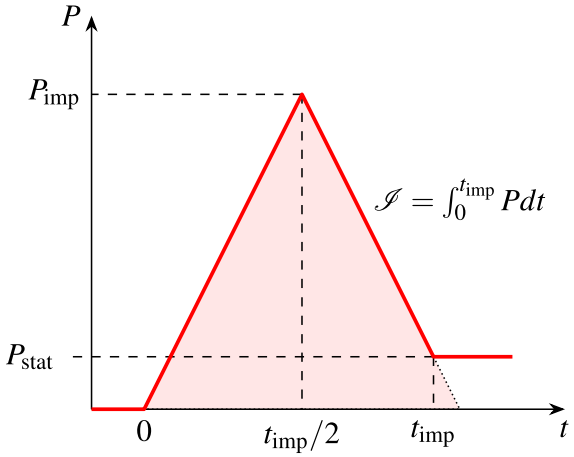

Fig. 4. Impulse relation from [23].

To determine the velocity and kinetic energy profiles, the following steps need to be performed:

(1) The velocity $v(x)$ is translated into kinetic energy $E_{\mathrm{k}}(x)$;
(2) At every impact location i the dissipated energy U_{v} and U_{s} is deducted from the kinetic energy $E_{\mathrm{k}}(x)$ in a step wise manner as described by Eq. (14);
(3) The resulting kinetic energy profile $E_{\mathrm{k}}(x)$ is translated back into a velocity profile $v(x)$ through Eq. (15); and finally,
(4) Distance travelled can be expressed into elapsed time t through numerical time integration.

As a result, the impact process is fully characterised in terms of velocity v, kinetic energy E_{k}, distance s, and time t. The relevant time instances of impact $t_{\mathrm{imp},1}$and $t_{\mathrm{imp},2}$ shown in Fig. 3 arise from the analysis for assessing successive column removals.

Modelling progressive collapse. The building structure subjected to vehicular impact was assessed using a nonlinear dynamic modelling framework for progressive collapse that supports both sequential and simultaneous damage scenarios involving single or multiple structural members. Developed in Python 3.10, it leverages the open-source finite element framework OpenSeesPy for its computational backend [24,25]. Detailed information about the framework's development, implementation, and failure criteria can be found in Cao et al. [26]. The structural characteristics are summarised in Table 3, where n_{pl} is the number of slotted-in shear plates in the timber connections with laterally loaded fasteners. General structural parameters such as surface load and span lengths are presented in Table 4. The acting surface load q_{Ed} is based on the accidental load combination $q_{\mathrm{Ed}} = (g_{\mathrm{k}} + \gamma_{\mathrm{t}}) + \psi_{2,1} q_{\mathrm{k}}$ according to EN 1990:2002 [27] with permanent loads g_{k}=3.00 kN/m^2, γ_{t}=1.00 kN/m^2, and variable loads q_{k}=3.00 kN/m^2.
For the simulation, a timber connection compromised of laterally loaded dowel-type fasteners and slotted-in steel plates is assumed. The hysteretic connection model is based on a linear elastic connection model with plastic hardening and damage accumulation [28]. Due to the limited ductility of conventional timber members, the ductility is often assumed to be concentrated in the connections [29]. A key parameter in the simulation is therefore the rotational capacity of the connections. Depending on the detailing of the timber connections, such connections often have low to moderate ductility μ, defined by the ratio between ultimate and yield displacement or rotation. Here, a ductility capacity of 6 is applied [30].

Table 3. Member design parameters.

Material (-)	Beam (mm)	Column (mm)	Connection (-)
GL24h	200 × 320	200 × 200	3 × 4Ø8 n_{pl}=2

Table 4. Structure design parameters.

Surface Load q_{Ed} (kN/m^2)	Load Coefficient $\psi_{2,1}$ (-)	Span-x (mm)	Span-y (mm)	Height-z (mm)
4.9	0.30	4000	4000	3500

Results and Discussion

Vehicular Impact. The velocity profile in Fig. 5a illustrates the deceleration of the lorry as it travels from the road to the second column within the building, where the initial velocities v_0 are depicted using a colour gradient. The first column is denoted by C1 and the second column by C2. Over the distance s, a linear and stepwise velocity reduction is observed. The stepwise velocity reduction occurs at the column location, whereas the linear velocity reduction is distributed along the distance. Velocity profiles with higher initial velocities are characterised by a smaller rate deceleration with respect to velocity profiles with lower initial velocities. The lower the initial velocity of the velocity profile, the higher the deceleration is characterised by a distinct parabolic reduction. As a reference parameter, the pre-impact velocity at the impact location is extracted from the calculation. Column C1 fails with a pre-impact velocity of v_{imp}=25.4 km/h while column C2 fails at v_{imp}=7.1 km/h. The second limit impact velocity v_{imp} is approximately 28% of the first one. Simulations between the two incidents C1 and C2 cross the zero-velocity-line, indicating a full arrest of the vehicle where others reach the column C2 without leading to further failure.

The time-dependent kinetic energy profile depicted in Fig. 5b showcases the reduction in energy during the deceleration and impact phases. To determine the kinetic energy, the velocity profile is scaled analogous to Eq. (16). Therefore, similar trends are observed, specifically, the continuous and sudden reduction in kinetic energy. The main difference is expressing the impact model in time instead of distance. This leads to a stretch of the x-axis between different kinetic energy profiles compared to the velocity profiles, as lower velocities require more time to travel the same distance. The sudden decrease is not vertical, as in the velocity profile, due to the time the vehicle interacts with the column at a certain location. This time is equivalent to the impact time t_{imp} which is in the order of 350 ms for column C1. From Fig. 5b the time delay between the collisions can be inferred. The time delay is visible by the plateau between the first and second collision. Depending on the post-impact velocity, a time delay in the range of 500 to 1500 ms is observed. This delay represents the time of travel until the vehicle reaches the second column. Higher initial velocities result in greater kinetic energy magnitudes and shorter time delays for successive impact.

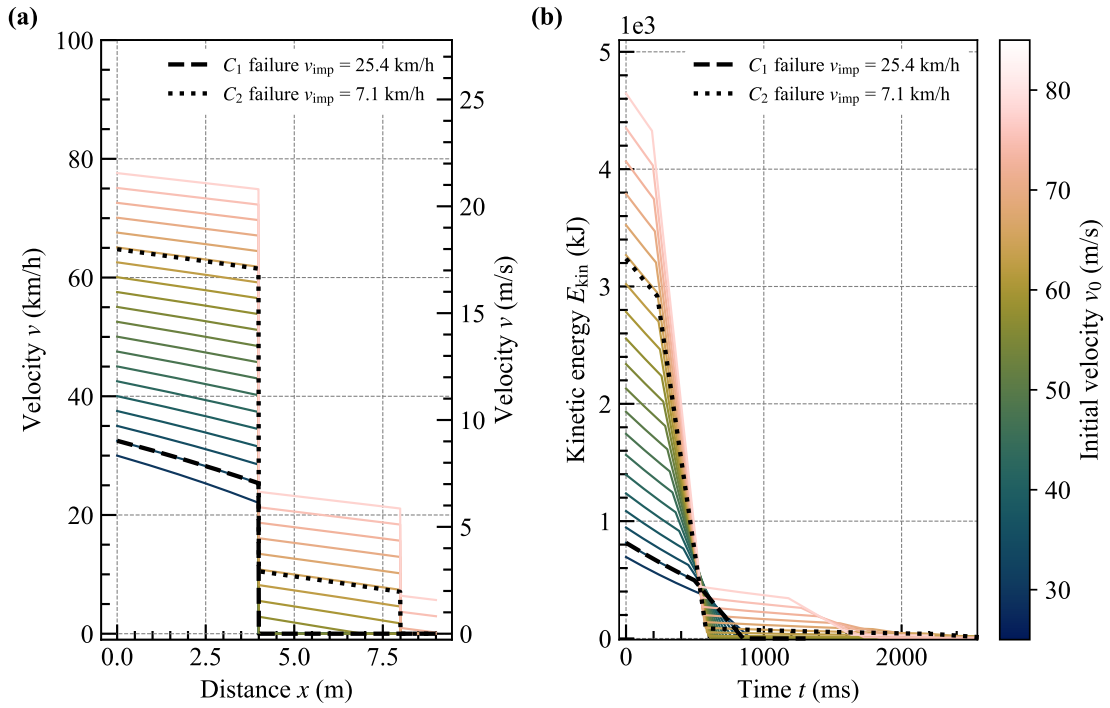

Fig. 5. Lorry simulation. (a) Velocity profile over distance travelled x. (b) Time-dependent kinetic energy profile.

The results confirm that higher initial velocities not only reduce the time interval between successive impacts but also result in the lorry retaining a greater residual velocity at each subsequent point of impact. This heightened residual velocity amplifies the likelihood of successive column failures if the members in question are not designed for impact loading. This highlights the critical influence of initial velocity in assessing vehicular impact on structures and mitigating the probability of successive failures.

Conventional design codes do not account for variable vehicle stiffness, the influence of the geometry of the impacted object and the vehicle type. With the framework presented in this paper, the aforementioned phenomena can be accounted for and is therefore physically coherent evaluation of vehicular impact. An important addition is the quantification of energy dissipation mechanisms. This enables system performance acceptance criteria that may be more cost-efficient than component-based acceptance criteria.

The damage characteristics of successive column failure are strongly dependent on the vehicular, trajectory, and structural parameters. For the assumed structure, impact location, and vehicle, successive column failure may occur if the lorry has an impact velocity v_{imp} of approximately 25.4 km/h or more. This corresponds to a kinetic energy E_{k} of about 498· kJ.

Vehicular Impact. The velocity profile in Fig. 5a illustrates the deceleration of the lorry as it travels from the road to the second column within the building, where the initial velocities v_0 are depicted using a colour gradient. The first column is denoted by C1 and the second column by C2. Over the distance s, a linear and stepwise velocity reduction is observed. The stepwise velocity reduction occurs at the column location, whereas the linear velocity reduction is distributed along the

Two progressive collapse simulations were conducted to evaluate the structural response for different damage scenarios. One progressive collapse simulation involved the removal of a single column, and the other included the removal of a second column at t=500 ms, designed to replicate the time delay in Fig. 5.

Fig. 6 shows the initial and final damage state of the structure following the removal of a single column. In this scenario, the structural configuration successfully arrested the propagation of further damage.

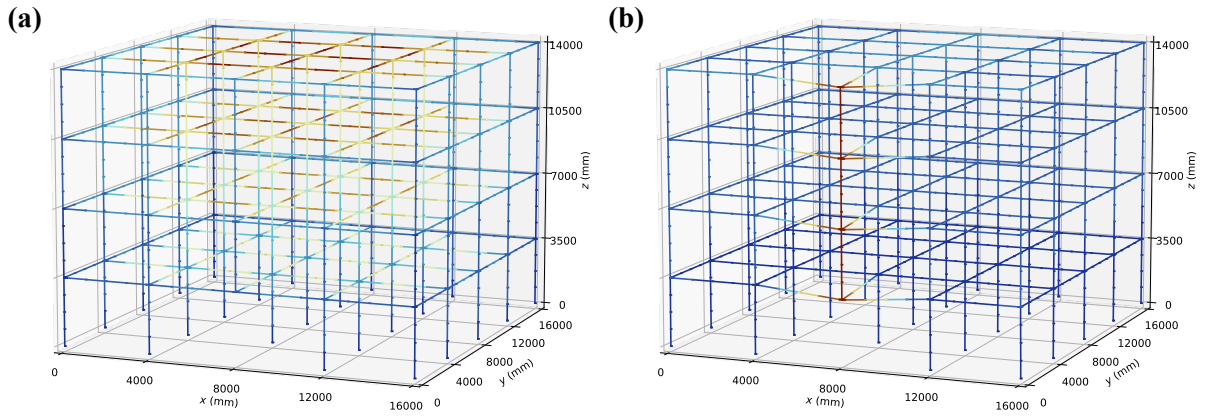

Fig. 6. Progressive collapse assessment of a frame structure subjected to the loss of a single column. (a) Initial damage state at t=0 ms (b) Final damage state.

Fig. 7 shows the initial and final damage state of the structure resulting from the successive column removal simulation. The final damage state reveals a complete failure of the compartments supported by the two removed columns. Fig. 8 provides further insight into the structural response following the initial column failure. The second column fails shortly after the peak rotational utilisation η_{rot} is reached. Between t=500 and 600 ms, the structure oscillates at larger amplitudes compared to the single column removal scenario. Beyond this point, rotational utilisation grows drastically, indicating a rapid loss of stability. Between t=600 and 800 ms many elements exceed the capacity, leading to their removal. By t=800 ms the structure reaches a steady or stationary state, signifying the conclusion of the failure process.

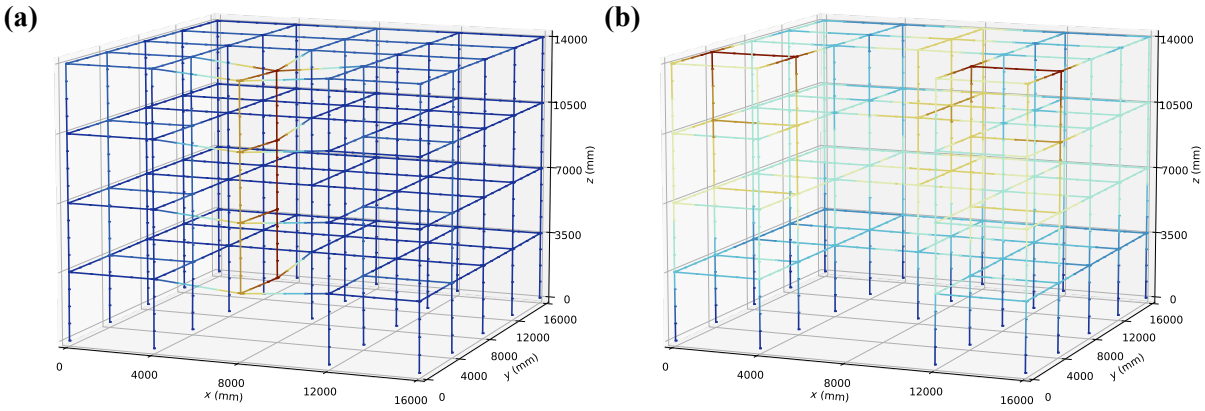

Fig. 7. Progressive collapse assessment of a frame structure subjected to the loss of multiple columns. (a) Secondary damage state at t=500 ms (b) Final damage state with compartment failure.

The maximum rotational utilisation η_{rot} in Fig. 8, reaches a peak value of approximately 5.60 at t=400 ms. Following this peak, the structure exposed to single column removal exhibits oscillatory behaviour, gradually stabilising without further increase in rotational demand. This indicates redundancy in the structure and therefore, the ability to effectively redistribute loads through alternate load paths. Alternate load paths can be ensured by enabling multiple load resisting mechanisms, such as bending and catenary action. To determine which load resisting mechanism dominates, the maximum vertical displacement can be analysed. The maximum vertical deflection Δ in the single column removal scenario is approximately 408 mm. If the stiffness of the connections is substantially lower than the beams, the beams adjacent to the removed column will mostly experience rigid-body

movement from the deflections [26]. Assuming rigid body movement, the rotation of the connection results in θ_{max}=0.102 rad. The elastic limit is approximately θ_{el}=0.018 rad. With a maximum rotation utilisation factor of 5.60 and a rotation ductility demand due to rigid body movement of θ_{max}/θ_{el}=5.66, the result indicates a substantial load carrying mechanism through catenary action.

The progressive collapse simulations highlight the significant difference in structural behaviour between single and successive column removals. The first simulation, involving the removal of a single column, demonstrates the building's ability to withstand localised failures without compromising overall integrity. Despite the initial disturbance, the building remains stable, with no further failures observed. This suggests that the load redistribution mechanisms within the structure can accommodate the localised loss of a column. In contrast, the second simulation with successive column removal reveals a different outcome. The secondary removal of a column designed to mimic the conditions of Fig. 5, triggers a progressive collapse. The initial column removal introduces significant stress redistribution, as evidenced by the peak rotational utilisation η_{rot}. However, the addition of a secondary failure pushes the structure beyond its capacity to redistribute loads effectively, resulting in a progressive collapse. These results highlight the compounding effects of successive column removals on structural integrity and stability.

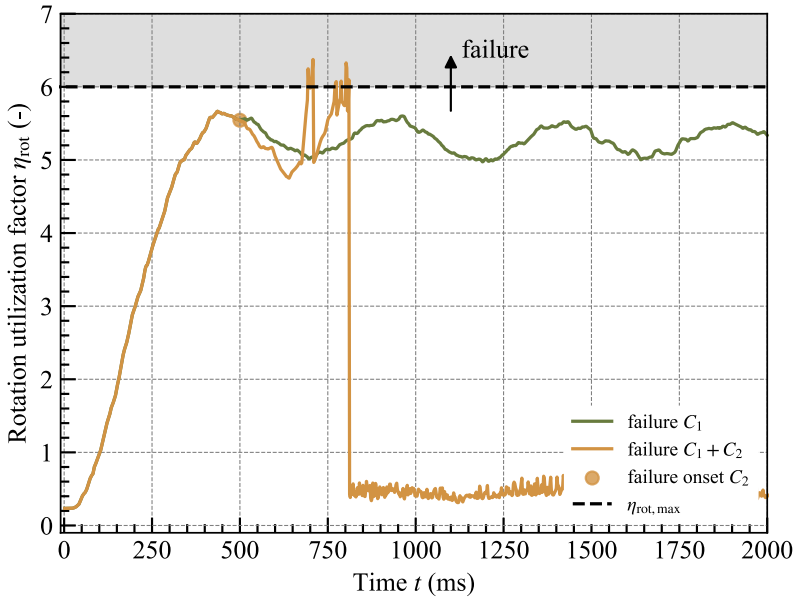

Fig. 8. Maximum rotation utilisation η_{rot} of the progressive collapse simulations.

Conclusions

Current robustness assessment methods are based on the notional removal of structural members or compartments. However, they may fail to capture damages, such as systematic errors and chained damage events. High-impulse vehicular impact may not be adequately represented using current methods, as they can result in successive losses of structural members. The growing number of vehicle-based attacks and accidents highlight the need to better understand and assess such hazard events. Conventional design approaches address vehicular impact using prescriptive forces and simplified models that overlook important physical phenomena, emphasising the need for more sophisticated models. In this study, the adequacy of notional damages for vehicular impacts on building structures is evaluated and a framework employing velocity and energy profiles is presented. The use of the framework is exemplified through a case study.

The velocity profiles and impact timing reveal the effects of vehicular impacts on building structures. In the case of a lorry impact, the model showed that secondary member failure following the original trajectory is possible and can be assessed from the kinetic energy of the vehicle and energy dissipation mechanisms. This requires models that account for vehicle deceleration, energy dissipation and propagating actions. The findings suggest that existing methods in practice

inadequately capture the necessary physical phenomena, necessitating more sophisticated methods for evaluating the risk of progressive collapse. The progressive collapse simulations reveal a significant difference between single and successive column removals. For a single column removal, the structure demonstrated sufficient capacity for load redistribution to prevent further failures. Successive column removal triggered a progressive collapse. The results suggest that while the structure can effectively resist the loss of a single column, the introduction of additional damage may lead to progressive collapse. This highlights the need for enhanced design strategies to mitigate risk of progressive collapse.

A limitation of this study is the assumption that the vehicular trajectory remains unaffected after the initial impact; in reality, eccentric impacts or deflected trajectories may occur, reducing the chance of reaching a second column. Additionally, no damage accumulation or force saturation was considered for the vehicles, with each impact having the same energy dissipating potential. Further studies should be conducted to assess the effect of the time delay on the damage to the second column. On the structural side, the axial loads in the column were not considered. This omission neglects resistance from inertia and the moment resistance that could arise from a compressive loading of the column. Another limitation is the removal of the column without directly simulating the introduction of the impulse to the structure. This approach disregards the energy transferred to the structure due to the impact. A comparison with empirical data and prescriptive values should be conducted to confirm the model assumptions.

This study underscores the importance of advancing progressive collapse assessments to address hazards, such as vehicular impacts. The findings reveal critical gaps in conventional methods, particularly in their inability to capture relevant physical phenomena. Design standards and guidelines should include more sophisticated methods that account for variable vehicle stiffness and energy dissipation mechanisms. This could lead to an adoption of performance-based design approaches on a system, rather than on a component level. Expanding this framework to diverse vehicular types, scenarios, and structural configurations will refine threat-specific progressive collapse evaluations.

Acknowledgments

The authors gratefully acknowledge the financial support provided by *MainWood*, a Joint Initiative co-financed by the ETH Board.

References

[1] European Committee for Standardization, EN 1991-1-7:2006. Eurocode 1: Actions on structures, General actions - Accidental actions, (2016).

[2] American Society of Civil Engineers, ASCE/SEI 76-23. Standard for Mitigation of Disproportionate Collapse Potential in Buildings and Other Structures, (2023).

[3] U.S. Army Corps of Engineers, Naval Facilities Engineering Systems Command, Air Force Civil Engineer Center, UFC 4-023-03. Design of Buildings to Resist Progressive Collapse, (2009). https://www.wbdg.org/ffc/dod/unified-facilities-criteria-ufc/ufc-4-023-03 (accessed October 7, 2024).

[4] University of Maryland, Global Terrorism Database, (2022). http://apps.start.umd.edu/gtd/ (accessed January 14, 2025).

[5] Storefront Safety Council, The most updated storefront crash database, (2023). https://www.storefrontsafety.org (accessed January 14, 2025).

[6] K. Wilson, Streetsblog USA, Vehicle-Into-Building Crashes 40% Higher Than Previously Thought, (2022). https://usa.streetsblog.org/2022/06/21/vehicle-into-building-crashes-40-higher-than-previously-thought (accessed January 14, 2025).

[7] D. Kronman, The Seattle Times, More drivers have been crashing into Seattle buildings, (2023). https://www.seattletimes.com/seattle-news/transportation/how-often-do-cars-crash-into-buildings-in-seattle-way-more-than-you-think/ (accessed January 14, 2025).

[8] A. Ateya, The Michigan Daily, Cars should not crash into buildings, (2023). http://www.michigandaily.com/opinion/cars-should-not-crash-into-buildings/ (accessed January 14, 2025).

[9] Norwegian Safety Investigation Authority, Investigation of tram derailment at the intersection between Nygata and Storgata in Oslo, (2024). https://nsia.no/Rail/Rail/Investigations/24-795 (accessed January 27, 2025).

[10] Redaktionsnetzwerk Deutschland, LKW-Unfall in Thüringen/Altkirchen: Gebäude stürzt ein, Fahrer stirbt, (2020). https://www.rnd.de/panorama/lkw-unfall-in-thuringenaltkirchen-gebaude-sturzt-ein-fahrer-stirbt-46Z75TD4YXZUZXJMJPVA6OLGMQ.html (accessed January 14, 2025).

[11] JCSS, Probabilistic Model Code: Part II - Load Models, Impact Load, Joint Committee on Structural Safety, 2001.

[12] A. Taushanov, E. Spasova, Determination of Vehicle Impact Loads according to different Design codes, Annu. Univ. Archit. Civ. Eng. Geod. Sofia 57 (2024) 739.

[13] K.L. Campbell, Energy Basis for Collision Severity, in: SAE International, 1974. https://doi.org/10.4271/740565.

[14] C. Bare, D. Peterson, M. Marine, K. Welsh, Energy Dissipation in High Speed Frontal Collisions, in: SAE International, 2013. https://doi.org/10.4271/2013-01-0770.

[15] N. Poirette, F.P. Bayan, J. Suway, A. Cornetto, A. Cipriani, R. Wahba, N. Poirette, F.P. Bayan, J. Suway, A. Cornetto, A. Cipriani, R. Wahba, Stiffness Coefficients of Heavy Commercial Vehicles, in: SAE International, 2013. https://doi.org/10.4271/2013-01-0796.

[16] H. Al-Thairy, Y.C. Wang, An assessment of the current Eurocode 1 design methods for building structure steel columns under vehicle impact, J. Constr. Steel Res. 88 (2013) 164–171. https://doi.org/10.1016/j.jcsr.2013.05.013.

[17] K.M.A. Sohel, K. Al-Jabri, A.H.S. Al Abri, Behavior and design of reinforced concrete building columns subjected to low-velocity car impact, Structures 26 (2020) 601–616. https://doi.org/10.1016/j.istruc.2020.04.054.

[18] European Committee for Standardization, EN 14080:2013. Glued laminated timber and glued solid timber - Requirements, (2016).

[19] A. Cao, A. Frangi, Dynamic strength increase of glued laminated timber beams subjected to impact loading, in: 2023. https://doi.org/10.3929/ethz-b-000653637.

[20] S. Schilling, P. Palma, R. Steiger, A. Frangi, Probabilistic description of the mechanical properties of glued laminated timber made from softwood, in: INTER Proc. Meet. Fifty-Four 2021, Timber Scientific Publishing, 2021: pp. 333–349. https://doi.org/10.3929/ethz-b-000505371.

[21] JCSS, Probabilistic Model Code: Part III - Resistance Models, Timber, Joint Committee on Structural Safety, 2006.

[22] A. Cao, P. Palma, A. Frangi, Dynamic amplification factors in instantaneously loaded structures, Eng. Struct. (2025).

[23] A. Cao, Modelling progressive collapse of timber buildings and its applications, Doctoral Thesis, ETH Zurich, 2024. https://doi.org/10.3929/ethz-b-000706559.

[24] F. McKenna, M.H. Scott, G.L. Fenves, Nonlinear Finite-Element Analysis Software Architecture Using Object Composition, J. Comput. Civ. Eng. 24 (2010) 95–107. https://doi.org/10.1061/(ASCE)CP.1943-5487.0000002.

[25] M. Zhu, F. McKenna, M.H. Scott, OpenSeesPy: Python library for the OpenSees finite element framework, SoftwareX 7 (2018) 6–11. https://doi.org/10.1016/j.softx.2017.10.009.

[26] A. Cao, L. Esser, A. Frangi, Modelling progressive collapse of timber buildings, Structures 62 (2024) 106279. https://doi.org/10.1016/j.istruc.2024.106279.

[27] European Committee for Standardization, EN 1990:2002. Eurocode: Basis of structural design, (2016).

[28] A. Cao, P. Palma, A. Frangi, Multi-scale hysteretic model of laterally loaded timber connections with dowel-type fasteners, in: 2023: pp. 915–926. https://doi.org/10.3929/ethz-b-000619274.

[29] K.A. Malo, J. Siem, P. Ellingsbø, Quantifying ductility in timber structures, Eng. Struct. 33 (2011) 2998–3006. https://doi.org/10.1016/j.engstruct.2011.03.002.

[30] M. Geiser, L. Furrer, L. Kramer, S. Blumer, M. Follesa, Investigations of connection detailing and steel properties for high ductility doweled timber connections, Constr. Build. Mater. 324 (2022) 126670. https://doi.org/10.1016/j.conbuildmat.2022.126670.

The publication of this article was funded by the ETH Zurich 10.13039/501100003006